Available online at www.sciencedirect.com
ScienceDirect
Trans. Nonferrous Met. Soc. China 34(2024) 3721−3736
Transactions of Nonferrous Metals Society of China
www.tnmsc.cn

Distribution behavior of valuable elements in oxygen-enriched top-blown smelting process of waste printed circuit boards

Kang YAN[1,2,3], Wen-can QUAN[1,2,3], Zhong-tang ZHANG[1,2,3], Hua-ping NIE[1,2,3], Rui-xiang WANG[1,2,3], Zhi-feng XU[2,3,4]

1. School of Metallurgy Engineering, Jiangxi University of Science and Technology, Ganzhou 341000, China;
2. Key Laboratory of Ionic Rare Earth Resources and Environment, Ministry of Natural Resources, Ganzhou 341000, China;
3. Ganzhou Engineering Technology Research Center of Green Metallurgy and Process Intensification, Ganzhou 341000, China;
4. School of Material Engineering, Jiangxi College of Applied Technology, Ganzhou 341000, China

Received 20 April 2023; accepted 15 November 2023

Abstract: Oxygen-enriched top-blown smelting is a promising technology for processing waste printed circuit boards (WPCBs). The distribution behavior of valuable elements in WPCBs during smelting was investigated by varying the oxygen-enriched concentration, oxygen volume, CaO/SiO_2 (mass ratio), and Fe/SiO_2 (mass ratio). The optimal operating conditions were obtained by implementing a one-factor-at-a-time method. X-ray diffractometer, scanning electron microscopy−energy dispersive spectrometer, and inductive coupled plasma-atomic emission spectroscopy methods were utilized to detect the chemical composition, occurrence state as well as elemental contents of alloy and slag. It is found that the elements of Cu, Sn and Ni are mainly accumulated in the alloy while Fe is mainly oxidized into the slag. The direct yields of Cu, Sn and Ni are 90.18%, 85.32% and 81.10% under the optimal conditions of temperature 1250 °C, oxygen-enriched concentration 30%, oxygen volume 24 L, CaO/SiO_2 mass ratio 0.55, and Fe/SiO_2 mass ratio 1.05. The results show that the valuable metals are mainly lost in the slag through mechanical entrainment.

Key words: waste printed circuit boards; top-blown smelting; element distribution; thermomechanical analysis; slag type

1 Introduction

With the rapid development of the electronics industry, the production of electronic waste has increased dramatically. The total amount of electronic waste generated globally is expected to reach 74 million tons by 2030. The continuous growth of waste printed circuit boards (WPCBs) not only leads to considerable wastage of metal resources, but also causes various environmental problems. Therefore, the comprehensive utilization of WPCBs is one of the current research hotspots [1−4].

At present, main treatment methods of WPCBs include mechanical, pyrolysis, hydrometallurgical, and pyrometallurgical technologies [5−9]. LIU et al [10] reported that the selective recovery of metal Cu in WPCBs can be realized by mechanochemical methods with high valence Fe salt during ball milling. HUANG et al [11] carried out acid leaching of WPCBs after microwave pyrolysis, and achieved 80% gold recovery rate. The mechanical treatment and pyrolysis processes

Corresponding author: Zhong-tang ZHANG, Tel: +86-797-8312422, E-mail: zhzhtg@163.com
DOI: 10.1016/S1003-6326(24)66636-7

have the advantages of low energy consumption and pollution, but the products obtained are mostly a mixture of non-metal particles, making the subsequent separation difficult. Hence, these methods are often only used as pretreatment processes [12].

Hydrometallurgical technology is widely used in the recovery of WPCBs [13]. GÁMEZ et al [14] studied the leaching of precious metals in the WPCBs using "$(NH_4)_2S_2O_3$+Cu^{2+}" system, and found that the leaching rate of gold reached 87%. LI et al [15] proposed a novel process for extracting precious metals from WPCBs under alkaline glycine-permanganate leaching system. The leaching rates of gold and copper reached more than 85% under the optimal conditions. Although hydrometallurgical technology has the advantages of low energy consumption and high recovery rate, it produces a large amount of wastewater during leaching [5,16].

Pyrometallurgical technology has attracted more and more attention from researchers due to its strong feedstock adaptability and large disposal capacity. Oxygen-enriched smelting technology is a typical modern intensive smelting process, with the features of low comprehensive energy consumption and high recovery rate of valuable metals. It plays an important role in the ore smelting and pyro-metallurgical recovery of secondary resources [17−19]. In recent years, the treatment of WPCBs by oxygen-enriched smelting technology has been reported [20−23]. GUO et al [24] explored the effect of slag type on the smelting of WPCBs, and found that the ideal slag type was SiO_2−CaO−Al_2O_3−FeO quaternary slag system. CHEN et al [25,26] recycled the precious metals and trace elements in waste electrical and electronic equipment at high P_{SO_2} and analyzed the distribution behaviors of main metal elements. ZHANG et al [23] investigated the fundamental theory of pyrometallurgical direct smelting of WPCBs and demonstrated that an alloy with high copper content can be obtained during smelting. In summary, oxygen-enriched top-blown smelting technology has significant advantages in the treatment of WPCBs. The direct yield and alloy grade of alloy are very important technical indicators during smelting, which can be determined by the distribution behavior of valuable elements. However, the current research is only focused on the thermodynamics and process conditions of the smelting process, and there are few studies on the distribution behavior of valuable elements during smelting [17,27,28].

In view of this, the distribution behavior of valuable elements in the oxygen-enriched top-blown smelting process of WPCBs was systematically investigated herein for the first time. This work can clarify the behavior and trends of valuable elements during smelting, which can improve the direct yield of metals in the smelting process. Moreover, it can provide theoretical guidance and technical support for the improvement of the pyrometallurgical treatment process of WPCBs.

2 Experimental

2.1 Materials

The WPCBs used in the experiment were obtained from a circuit board recycling plant in Shanghai, and the main components are listed in Table 1. The contents of Cu, Fe, Sn and Ni are 37.75 wt.%, 17.88 wt.%, 3.28 wt.% and 3.23 wt.%, respectively. The XRD pattern of WPCBs is shown in Fig. 1(a), and the main phases consist of Cu, Fe, Sn, SiO_2 and Al_2O_3. The water-quenched slag from Henan Yuguang Gold & Lead Co., Ltd., China, after fuming was utilized as a slagging agent, and its main components are listed in Table 2. Based on its XRD pattern (see Fig. 1(b)), the main phases in the water-quenched slag include FeO, SiO_2, Al_2O_3 and $CaSiO_3$. The analytical pure reagents of CaO (98.0 wt.%, Sinopharm) and SiO_2 (99.0 wt.%, Sinopharm) were utilized to adjust the slag phase composition. Industrial pure oxygen and nitrogen (99.0 wt.%, Ganzhou Jianli Gas Company) were used to control the oxygen concentration and oxygen volume during smelting.

2.2 Experimental procedures and methods

Before the experiment, phase diagram, equilib and viscosity modules and FToxid databases in the

Table 1 Elemental analysis of WPCBs (wt.%)

Cu	Fe	Sn	Ni	Pb	Bi
37.75	17.88	3.28	3.23	0.18	0.01
SiO_2	Al_2O_3	CaO	Au	Ag	
9.45	2.90	1.98	0.02	0.19	

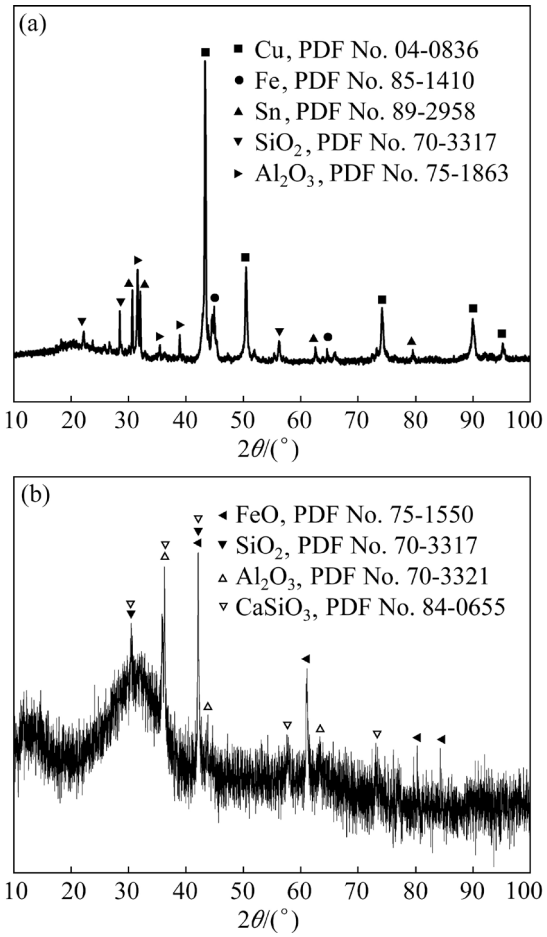

Fig. 1 XRD patterns of WPCBs (a) and water-quenched slag (b)

Table 2 Elemental analysis of water-quenched slag (wt.%)

Fe	Cu	Sn	Ni	Pb
33.08	0.19	0.11	0.02	0.13
SiO_2	Al_2O_3	CaO	MgO	Zn
27.88	8.35	8.98	2.03	2.03

thermodynamic software FactSage 7.3 were used to calculate the slag type range and smelting temperature [29,30]. First, 200 g WPCBs powder and 1500 g slag (CaO, SiO_2 and water-quenched slag) were weighed and mixed in an alundum crucible (3000 mL, 14 cm inner diameter, 20 cm height). Next, the crucible was placed into an electric furnace. The schematic diagram of the experimental device is shown in Fig. 2. Oxygen-enriched gas was injected into the slag via an alundum tube (6 mm inner diameter, 10 mm external diameter, 100 cm length) from the furnace top. The alundum tube was about 2 cm away from the bottom of the slag. The heating rate was set to be 5 °C/min, and the furnace temperature was raised to 1250 °C for 1 h to ensure the melting of the raw material. After reaction for 1 h, the crucible was allowed to stand for 40 min and cooled to room temperature in air. Finally, the alloy and smelting slag were weighed and analyzed.

The element distribution rates of Cu, Sn and Ni in the alloy and slag were calculated by Formulas (1) and (2), and the proportion of each metal in the alloy was calculated by Formula (3).

$$D_a = \frac{w_{Me} m_A}{m_{Me,tot}} \times 100\% \quad (1)$$

$$D_s = 1 - D_a \quad (2)$$

$$w_{Me} = \frac{m_{Me}}{m_A} \times 100\% \quad (3)$$

where D_a and D_s represent the distribution proportions of metal elements in the alloy and slag, respectively; w_{Me} is the mass fraction of metal elements in the alloy; m_A is the mass of the alloy; m_{Me}, and $m_{Me,tot}$ are the total mass of the metal Me in the alloy and raw material, respectively.

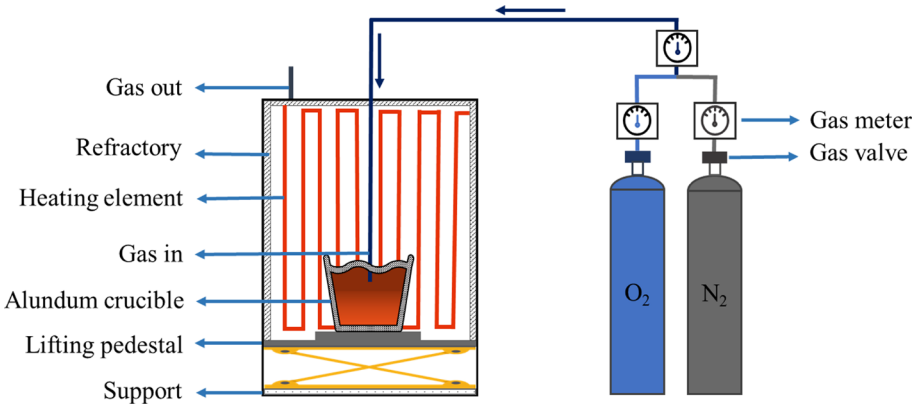

Fig. 2 Schematic diagram of experimental device

2.3 Analysis and testing

The chemical analysis of the main metal elements in the alloy and slag was performed by inductively coupled plasma-atomic emission spectroscopy (ICP-AES, Agilent 725, ICAP700, China). The phases of raw materials and smelting products were detected by X-ray diffractometer (XRD, Cu K_α, λ=0.154056 nm; Rigaku-TTR III, Japan). Scanning electron microscopy (SEM, JSM−6360LV, USA) and energy dispersive spectrometry (EDS, EDX-GENESIS 60 S, USA) were utilized to characterize the microstructure morphology and elemental composition of the smelting products. The analytical settings had an accelerating voltage of 20 kV and a working distance of 11 mm.

3 Results and discussion

3.1 Slag type selection

The slag properties are determined by slag type, which is an important factor affecting the smooth progress of the smelting process [24]. According to the composition characteristics of raw materials, Al_2O_3−SiO_2−FeO−CaO−1.5%MgO slag system was proposed. The phase diagram of the slag system is shown in Fig. 3.

As shown in Fig. 3(a), the liquid phase zone of Al_2O_3−SiO_2−FeO−CaO−1.5%MgO slag system expands with the increase of temperature. When the smelting temperature is 1150 °C, the slag liquid phase zone is small, which is mainly formed by the melting of ferric silicate. The slag liquid phase zone expands to the Al_2O_3−SiO_2 side and the Al_2O_3−FeO side as the temperature increases. Since the increase of Al_2O_3 content enhances the viscosity of slag and affects the fluidity of slag, the Al_2O_3 content should be controlled within the appropriate range during smelting [20]. Moreover, too high or too low Fe/SiO_2 mass ratio in slag would have a great impact on the liquid phase region area, which is not conducive to the smelting process. The liquidus of slag is more densely distributed at lower or higher Fe/SiO_2 ratios. That is, when the Fe/SiO_2 ratio is varied within a small range, the melting temperature of slag changes greatly, which is not conducive to the control of smelting conditions. As shown in the red zone of Fig. 3(b), the slag composition is in the liquid phase zone of the phase diagram under the conditions of Fe/SiO_2 ratio (0.75−1.25):1, Al_2O_3 content 5−10 wt.%, and smelting temperature 1150−1350 °C. In addition, the black-framed zone *ABCD* represents the actual slag composition. It can be observed that the actual slag composition is located within the red zone and within the 1200 °C isotherm line, indicating that the melting temperature of the actual slag composition is below 1200 °C.

The slag fluidity is determined by slag viscosity in the smelting process, which can affect the separation of metal and slag. When the slag viscosity is too large, the separation of metal and slag is poor, which reduces the metal recovery rate. Figure 4 shows the effects of Fe/SiO_2 and CaO/SiO_2 ratios on slag viscosity. It can be seen that the slag viscosity is less than 0.5 Pa·s when the smelting temperature is higher than 1200 °C with CaO/SiO_2 ratio of 0.35−0.65 and Fe/SiO_2 ratio of 0.85−1.15. At this time, the slag has good fluidity, which can ensure the smooth progress of the smelting process.

Based on the above analysis, the subsequent experiments were carried out under the conditions

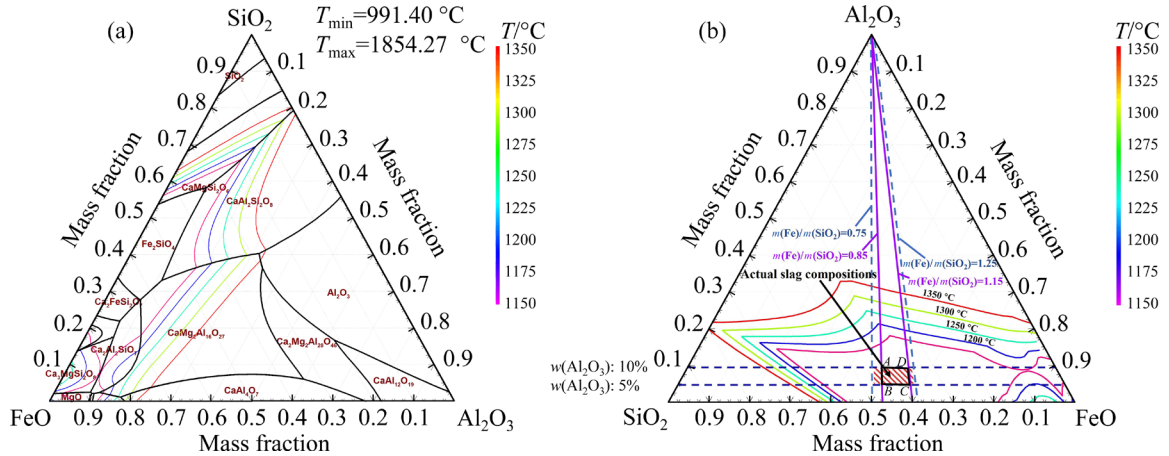

Fig. 3 Phase diagram of Al_2O_3−SiO_2−FeO−CaO−1.5%MgO slag system (p_{O_2}=1×10^{-5} Pa): (a) Phase diagram of slag system; (b) Slag type selection

of CaO/SiO_2 ratio 0.35−0.65, Fe/SiO_2 ratio 0.85−1.15, and smelting temperature 1250 °C.

3.2 Distribution behavior of valuable elements in oxygen-enriched top-blown smelting process of WPCBs

3.2.1 Effect of oxygen-enriched concentration

Figure 5 shows the effect of oxygen-enriched concentration on the distribution rates and direct yields of Cu, Sn and Ni. As shown in Figs. 5(a) and (b), the distribution rates and direct yields of Cu, Sn and Ni in the alloy increased with the increase of oxygen-enriched concentration. When the oxygen-enriched concentration increased from 30% to 60%, the distribution rates of Cu, Sn and Ni in the alloy increased from 67.57%, 58.93% and 64.80% to 95.78%, 96.50% and 90.49%, respectively. In addition, the content of impurity Fe in the alloy

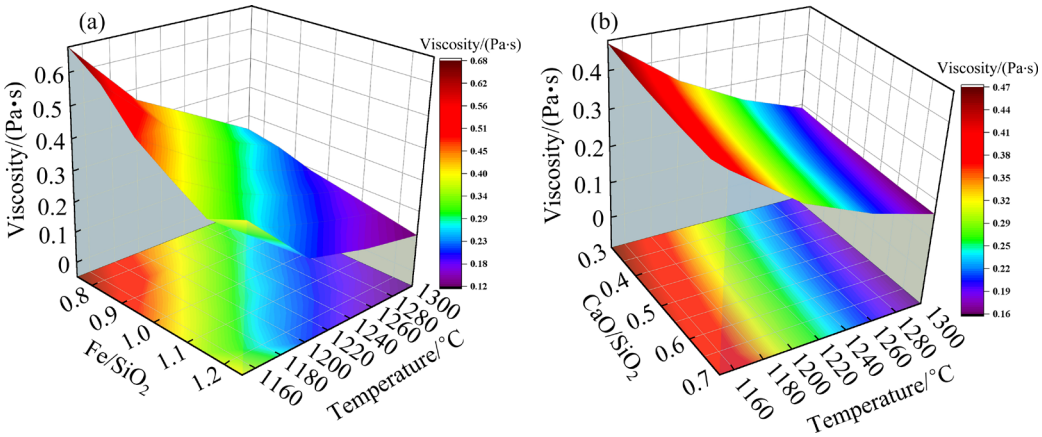

Fig. 4 Effect of Fe/SiO_2 ratio (a) and CaO/SiO_2 ratio (b) on slag viscosity at 1150−1300 °C (Al_2O_3=5.5 wt.%, Fe/SiO_2=0.75−1.25, CaO/SiO_2=0.3−0.7)

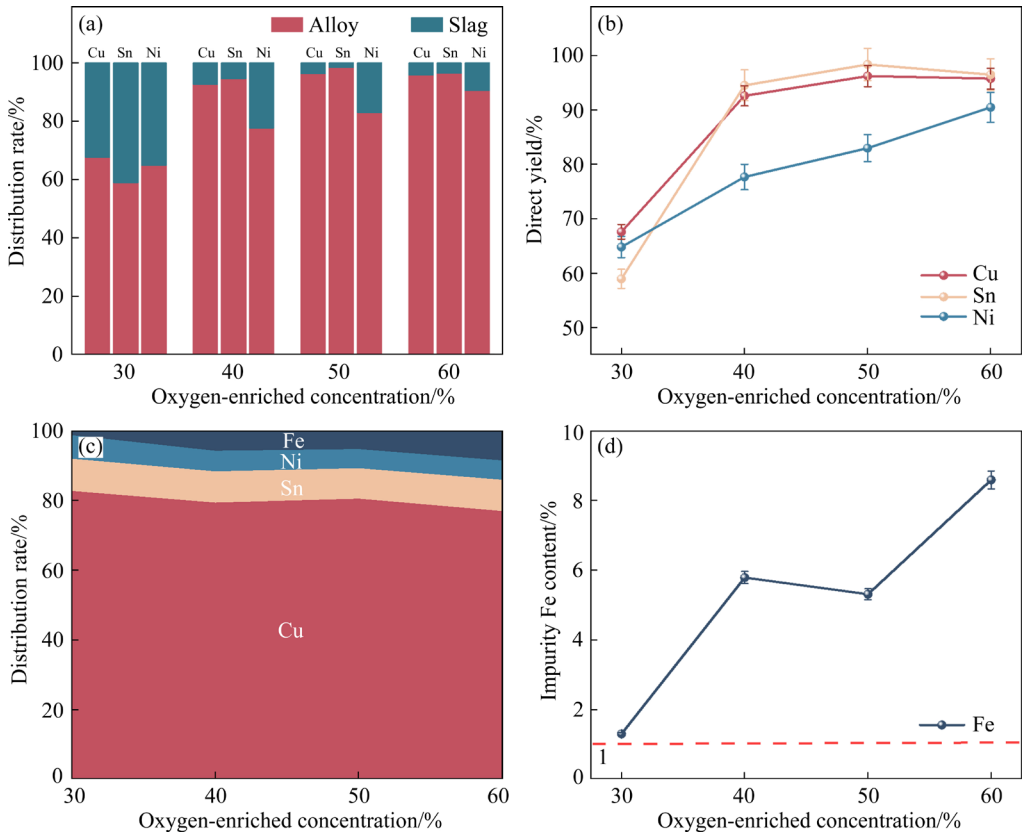

Fig. 5 Effect of oxygen-enriched concentration: (a) Distribution rates of Cu, Sn and Ni; (b) Direct yields of Cu, Sn and Ni; (c) Element distribution rate; (d) Impurity iron content (Smelting temperature 1250 °C, smelting time 1 h, oxygen volume 48 L, CaO/SiO_2 ratio 0.55, Fe/SiO_2 ratio 1.05)

increased rapidly (Figs. 5(c, d)), resulting in a significant decrease in the purity of the alloy. The main reason was the constant total oxygen volume during smelting. When the oxygen-enriched concentration is low, the total gas volume is large and the molten pool is fully stirred, which makes Fe easier to oxidize into the slag. On the contrary, when the oxygen-enriched concentration is high, the total gas volume is small and Fe cannot fully oxidize and partially enters the alloy phase, resulting in reducing the alloy grade.

Figure 6 presents the backscattered electron (BSE) and EDS analysis results of the alloy and slag at different oxygen-enriched concentrations. As seen from Figs. 6(a−d), when the oxygen-enriched concentration was 30%, the metal Sn was embedded

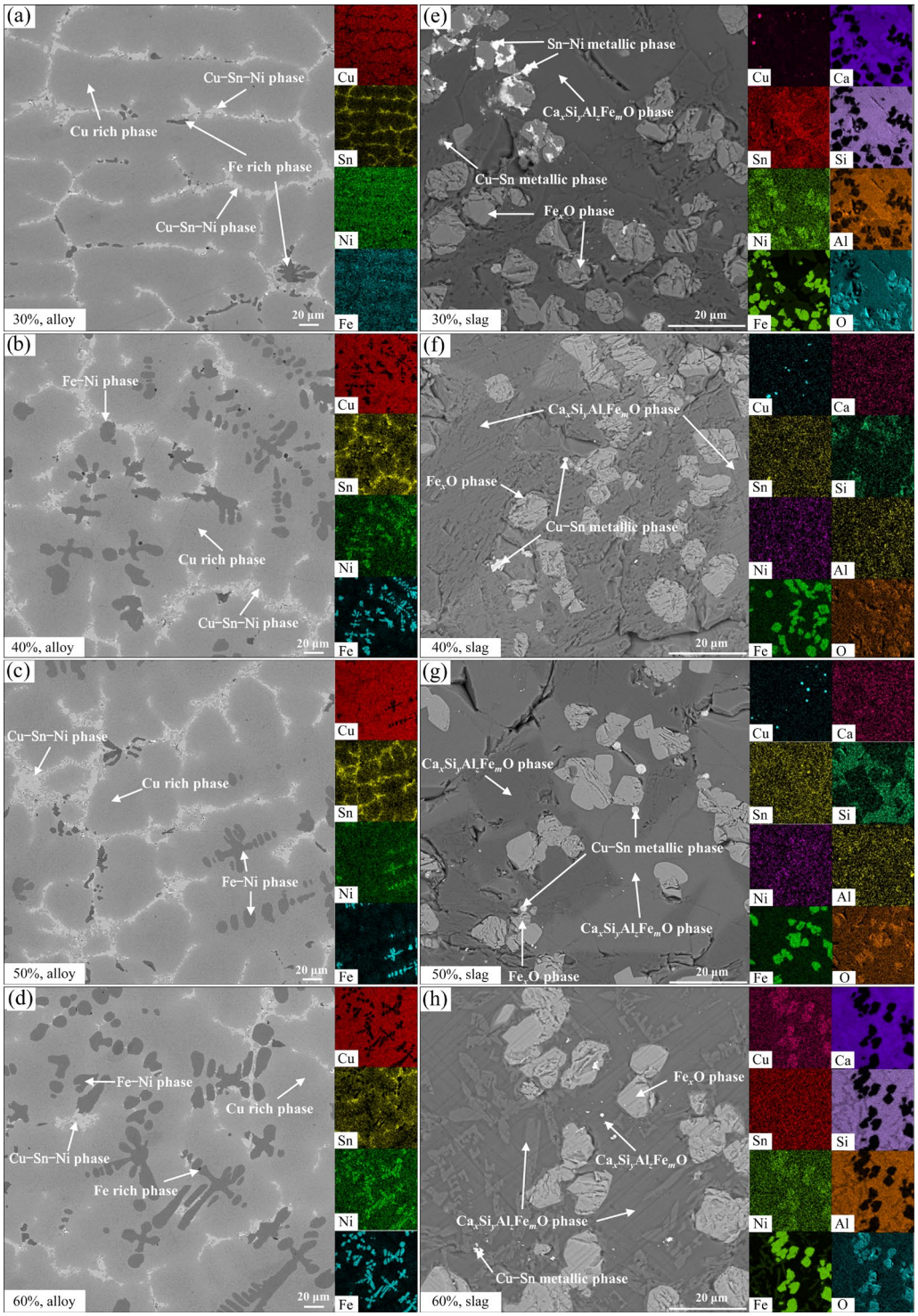

Fig. 6 BSE and EDS images of alloy (a−d) and slag (e−h) at various oxygen-enriched concentrations

in the Cu matrix while the metal Ni and a small amount of impurity Fe were uniformly dispersed in the alloy. Fe in the alloy cannot be fully oxidized into the slag with the increase of oxygen-enriched concentration, leading to the embedding of Fe and Ni in the alloy. Moreover, the area of the dark gray Fe−Ni phase dendrite region increased significantly while the area of the gray-white Cu−Sn−Ni phase band region decreased with the increase of oxygen-enriched concentration. This further confirmed that excessive oxygen concentration can increase the impurity content in the alloy due to insufficient stirring during smelting. As shown in Figs. 6(e−h), the slag was mainly composed of $Ca_xSi_yAl_zFe_mO$ silicate phase (large dark black area), Fe_xO phase (light gray blocky area), and Cu−Sn−Ni metal phase (light bright area).

From the above analysis, the content of impurity Fe in the alloy was only 1.3% when the oxygen-enriched concentration was 30%, which indicates the effective separation of Fe and valuable metals. On the contrary, although the direct yields of Cu, Sn and Ni increased, the impurity Fe content in the alloy was high at oxygen-enriched concentration beyond 30%. Therefore, the appropriate oxygen-enriched concentration was 30% to ensure the purity of the alloy obtained during smelting.

3.2.2 Effect of oxygen volume

Figure 7 shows the effect of oxygen volume on the distribution rates and direct yields of Cu, Sn and Ni. As seen in Figs. 7(a) and (b), the distribution rates and direct yields of Cu, Sn and Ni in the alloy decreased with the increase in oxygen volume, which suggested that the valuable metals were gradually oxidized into the slag. Figures 7(c) and (d) show that the Cu content in the alloy increased first and then decreased while Sn showed the opposite trend as oxygen volume increased. Moreover, the Ni content fluctuated in the range of 5%−7%, and the Fe content decreased from 7.15% to less than 1%. When the oxygen volume was low, the impurity element Fe in the alloy was insufficiently oxidized, resulting in a high Fe content in the alloy. With the

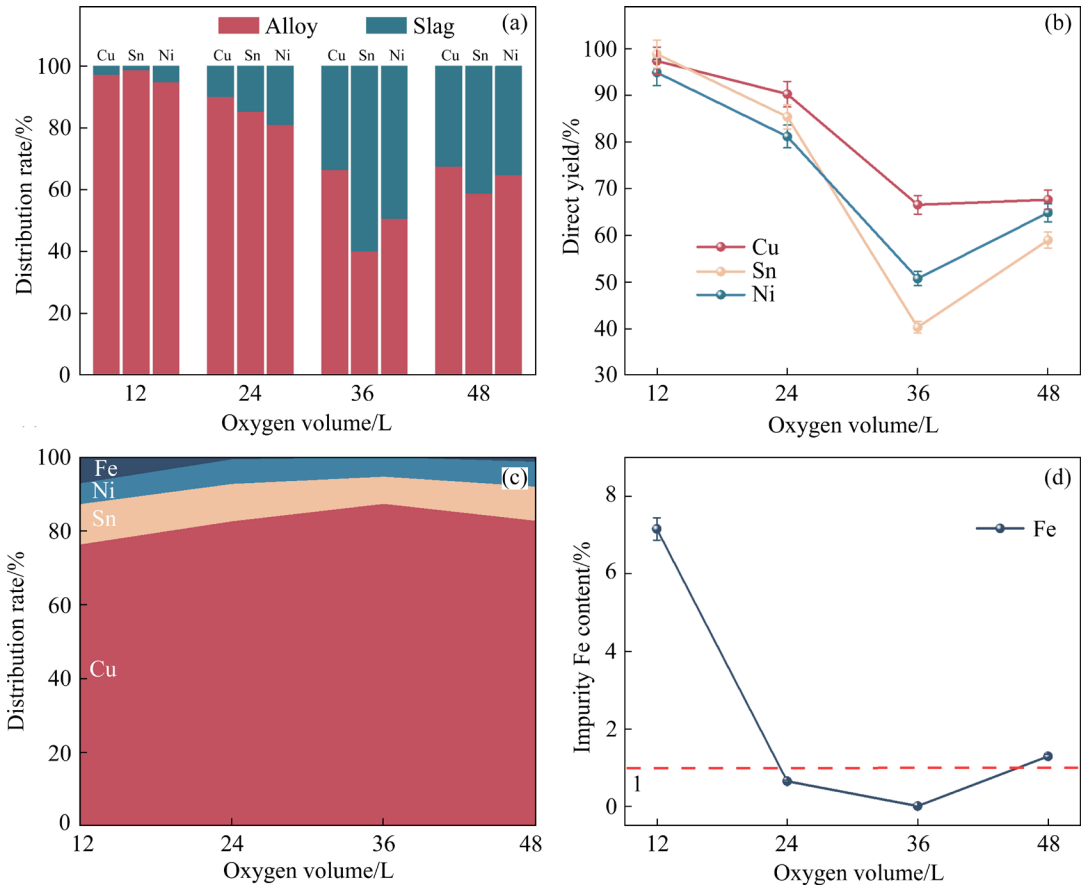

Fig. 7 Effect of oxygen volume: (a) Distribution rates of Cu, Sn and Ni; (b) Direct yields of Cu, Sn and Ni; (c) Element distribution rate; (d) Impurity iron content (Smelting temperature 1250 °C, smelting time 1 h, oxygen-enriched concentration 30%, CaO/SiO_2 ratio 0.55, Fe/SiO_2 ratio 1.05)

increase in oxygen volume, a large amount of Cu in the alloy was lost in the slag while the loss of Sn and Ni was low, resulting in a decrease in Cu content and a small increase of Sn and Ni in the alloy.

Figure 8 presents the BSE and EDS images of alloy and slag obtained at different oxygen volumes. The dark gray dendritic region of Fe−Ni phase with high Fe content and the gray white band region of Cu−Sn−Ni phase with high Sn−Ni content in the alloy (Figs. 8(a−d)) gradually decreased while the bright spot region of Cu−Sn phase in the slag (Figs. 8(e−h)) gradually increased with the increase of oxygen volume. This implied that more valuable

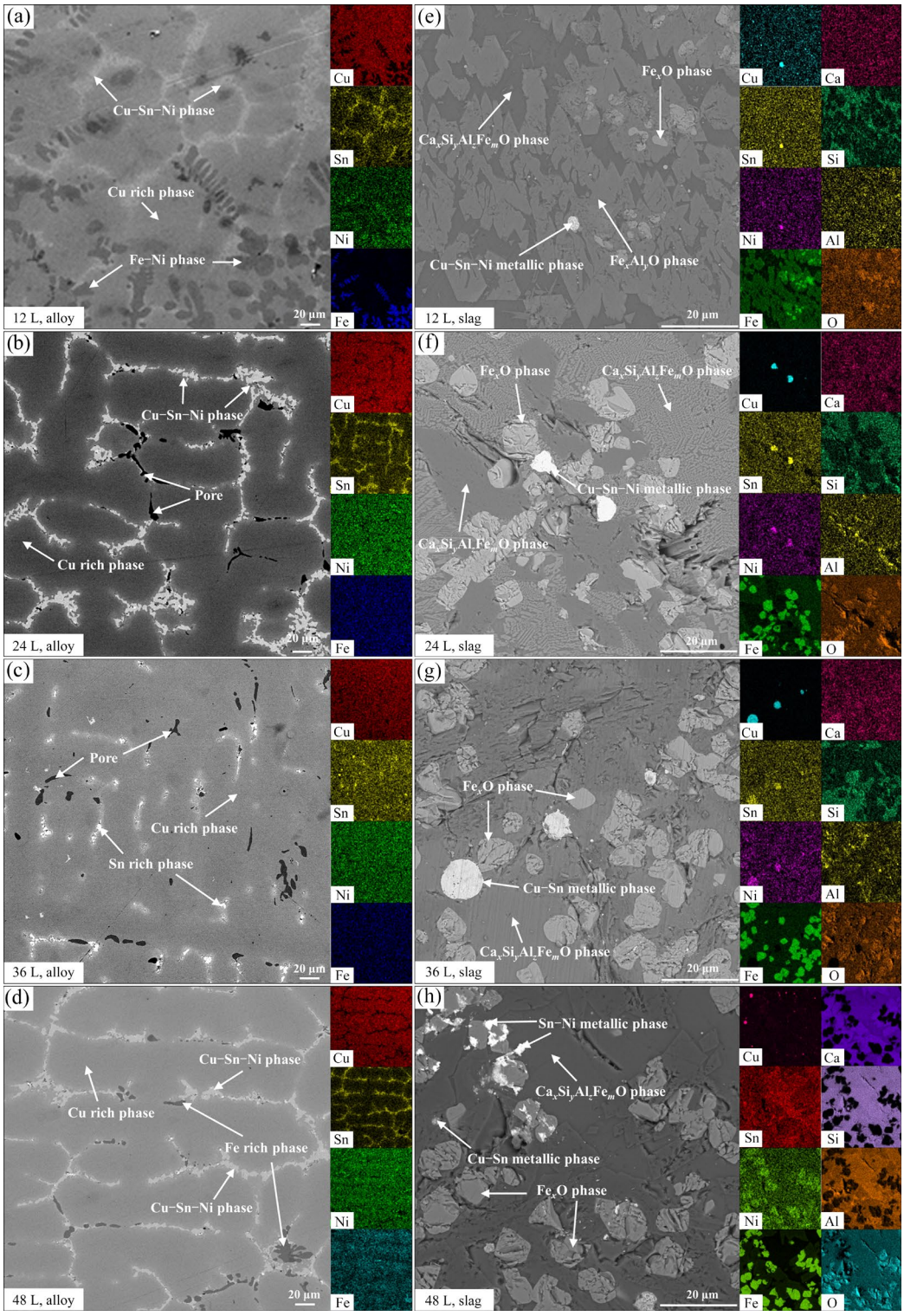

Fig. 8 BSE and EDS images of alloy (a−d) and slag (e−h) at different oxygen volumes

metals were lost in the slag phase. When the oxygen volume increased to 24 L, the accumulation area of Fe in the EDS images of alloy disappeared, indicating that most of the impurities were oxidized into the slag. At this moment, Sn was inlaid in the Cu matrix and Ni was dispersed in the alloy. EDS images of slag showed that metallic Cu, Sn and Ni in the slag mainly existed in the form of Cu−Sn−Ni phase in the right white spot region when the oxygen volume increased, indicating the loss of valuable metals in the slag by mechanical entrainment. Considering the purity of the alloy and the recovery rate of valuable metals, the oxygen volume of 24 L was considered to be appropriate.

3.2.3 Effect of CaO/SiO_2 ratio

Figure 9 shows the effect of CaO/SiO_2 ratio on the distribution rates and direct yields of Cu, Sn and Ni. As shown in Figs. 9(a) and (b), the distribution rates and direct yields of Cu, Sn and Ni in the alloy increased with the increase of CaO/SiO_2 ratio. This implied that the alloy and slag were difficult to separate when the CaO/SiO_2 ratio was lower, leading to a large amount of valuable metals in the slag. The slag viscosity decreased gradually as the CaO/SiO_2 ratio increased, which was beneficial to metal deposition and augmenting the direct yield of valuable metal. Figures 9(c) and (d) show that the increase in CaO/SiO_2 ratio was beneficial to enhancing the distribution of Sn and Ni in the alloy, while it had little effect on the Fe content in the alloy.

Figure 10 shows the BSE and EDS images of the alloy and slag obtained at different CaO/SiO_2 ratios. As seen in Figs. 10(a−d), the distribution of Sn and Ni in the alloy (gray band region of Cu−Sn−Ni phase in BSE images) changed from dispersion to aggregation with the increase in CaO/SiO_2 ratio. This further confirmed that the increase in CaO/SiO_2 ratio was conducive to improving the direct yield of alloy. As seen from Figs. 10(e−h), the smelting slag mainly consisted of $Ca_xSi_yAl_zFe_mO$ silicate phase, Fe_xO phase, and Cu−Sn−Ni metal phase. The bright white aggregation area of valuable metal in the slag significantly

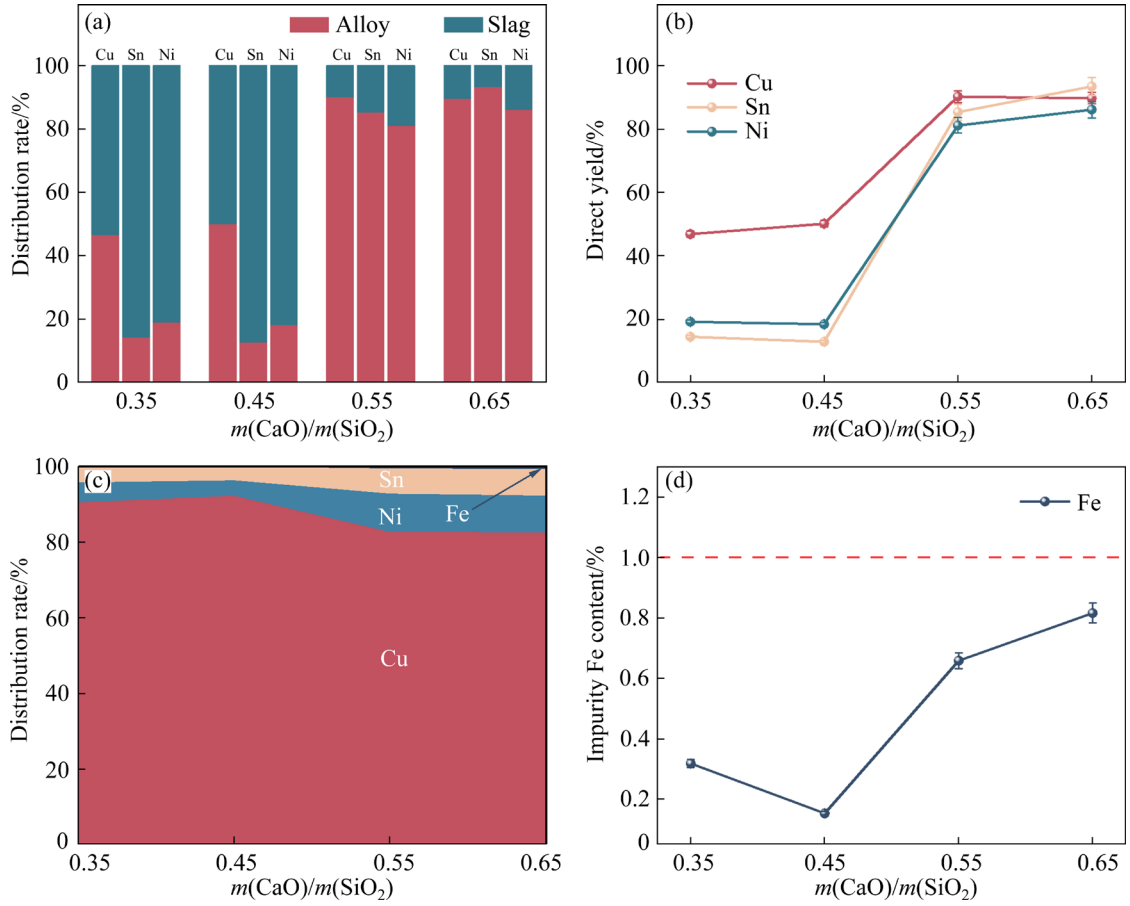

Fig. 9 Effect of CaO/SiO_2 ratio: (a) Distribution rates of Cu, Sn and Ni; (b) Direct yield of Cu, Sn and Ni; (c) Element distribution rate; (d) Impurity iron content (Smelting temperature 1250 °C, oxygen volume 24 L, smelting time 1 h, oxygen-enriched concentration 30%, Fe/SiO_2 ratio 1.05)

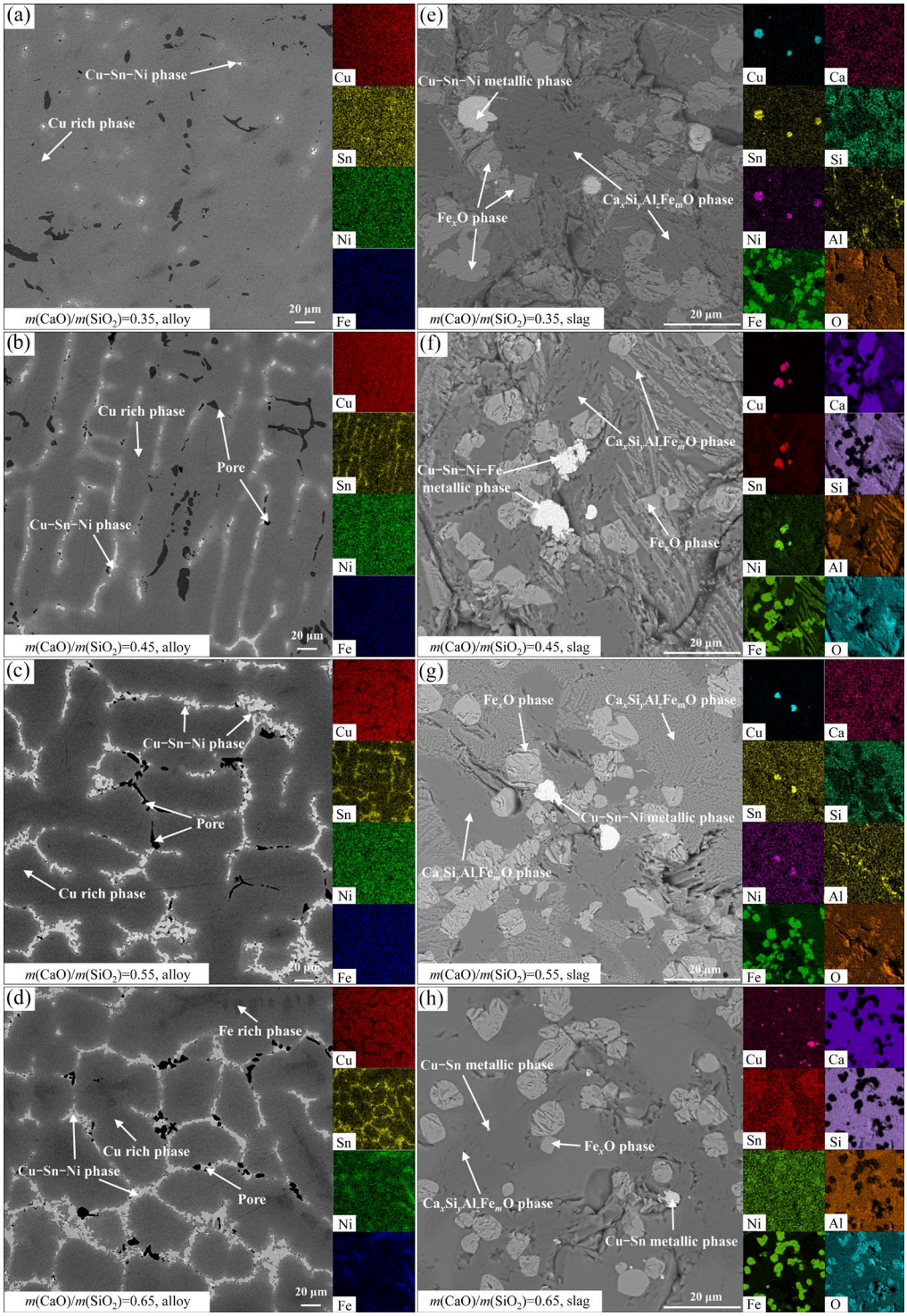

Fig. 10 BSE and EDS images of alloy (a−d) and slag (e−h) at different CaO/SiO_2 ratios

diminished when the CaO/SiO_2 ratio was higher than 0.45, demonstrating that the slag property can be improved by increasing the CaO/SiO_2 ratio in slag during smelting. In summary, considering the direct yield and purity of alloy, the CaO/SiO_2 ratio of 0.55 was determined to be appropriate.

3.2.4 Effect of Fe/SiO_2 ratio

Figure 11 shows the effect of Fe/SiO_2 ratio on the distribution rates and direct yields of Cu, Sn and Ni. The distribution rates and direct yields of Cu, Sn and Ni in the alloy decreased while the proportion of valuable metals in the alloy increased with the increase in Fe/SiO_2 ratio, which was

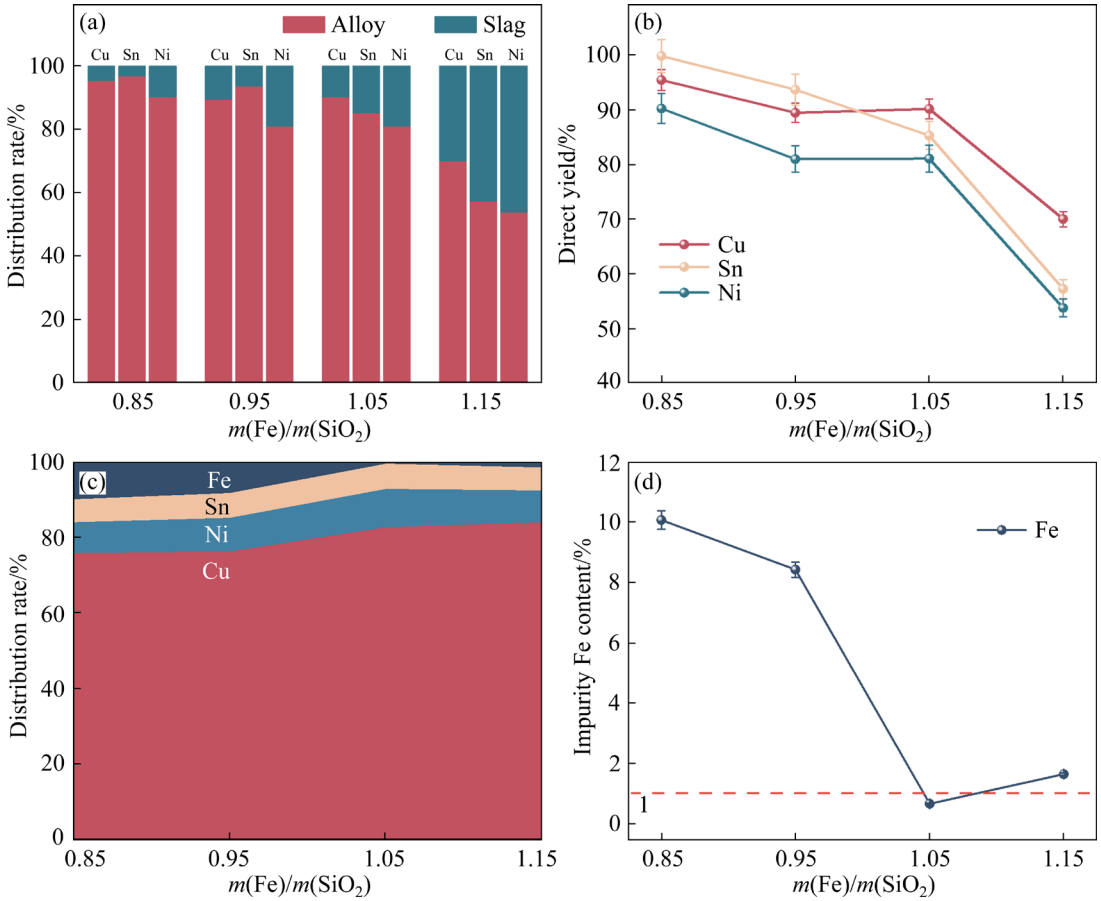

Fig. 11 Effect of Fe/SiO_2 ratio: (a) Distribution rates of Cu, Sn and Ni; (b) Direct yields of Cu, Sn and Ni; (c) Element distribution rate; (d) Impurity iron content (Smelting temperature 1250 °C, oxygen volume 24 L, smelting time 1 h, oxygen-enriched concentration 30%, CaO/SiO_2 ratio 0.55)

conducive to improving the purity of alloy. When the Fe/SiO_2 ratio increases from 0.85 to 1.05, the distribution rates of Cu, Sn and Ni in the alloy decreased from 95.47%, 96.86% and 90.27% to 90.18%, 85.32% and 81.10%, respectively. Moreover, the content of impurity Fe in the alloy decreased from 10% to less than 1%. When the Fe/SiO_2 ratio continued to increase, the direct yield of valuable metal decreased significantly and the impurity Fe content in the alloy increased slightly. This was because when the Fe/SiO_2 ratio was less than 1.05, the slag fluidity was poor due to the high melting temperature of slag. Moreover, although the distribution rates and direct yields of Cu, Sn and Ni in the alloy were high, Fe in the alloy could not be fully oxidized into the slag, which reduced the purity of the alloy. The increase in Fe/SiO_2 ratio can decrease the slag viscosity and improve slag fluidity, which is beneficial to metal deposition. However, the distribution rates and direct yields of valuable metal in the alloy decreased significantly when the Fe/SiO_2 ratio further increased. The main reason was that when the FeO content in the slag is appropriate, low melting point compounds ($2FeO{\cdot}SiO_2$ or $CaO{\cdot}FeO{\cdot}2SiO_2$) were formed by FeO with SiO_2 and CaO in the slag. However, SiO_2 and CaO contents were not enough to combine with FeO to form low melting point compounds when FeO was excessive, and the high melting point material FeO (1369 °C) can make the slag melting temperature rise sharply [23].

Figure 12 presents the BSE and EDS images of the alloy and slag at various Fe/SiO_2 ratios. As shown in Figs. 12(a−d), the element Fe mainly occurred in the dark gray dendritic region (Fe−Ni phase) of the alloy while Sn and Ni mainly existed in the gray-white band region (Cu−Sn−Ni phase) when the Fe/SiO_2 ratio was small. The distribution region of Fe−Ni phase in the BSE image of the alloy was obviously reduced and the Fe content in the alloy also decreased as Fe/SiO_2 ratio increased, which confirmed that the increase in Fe/SiO_2 ratio

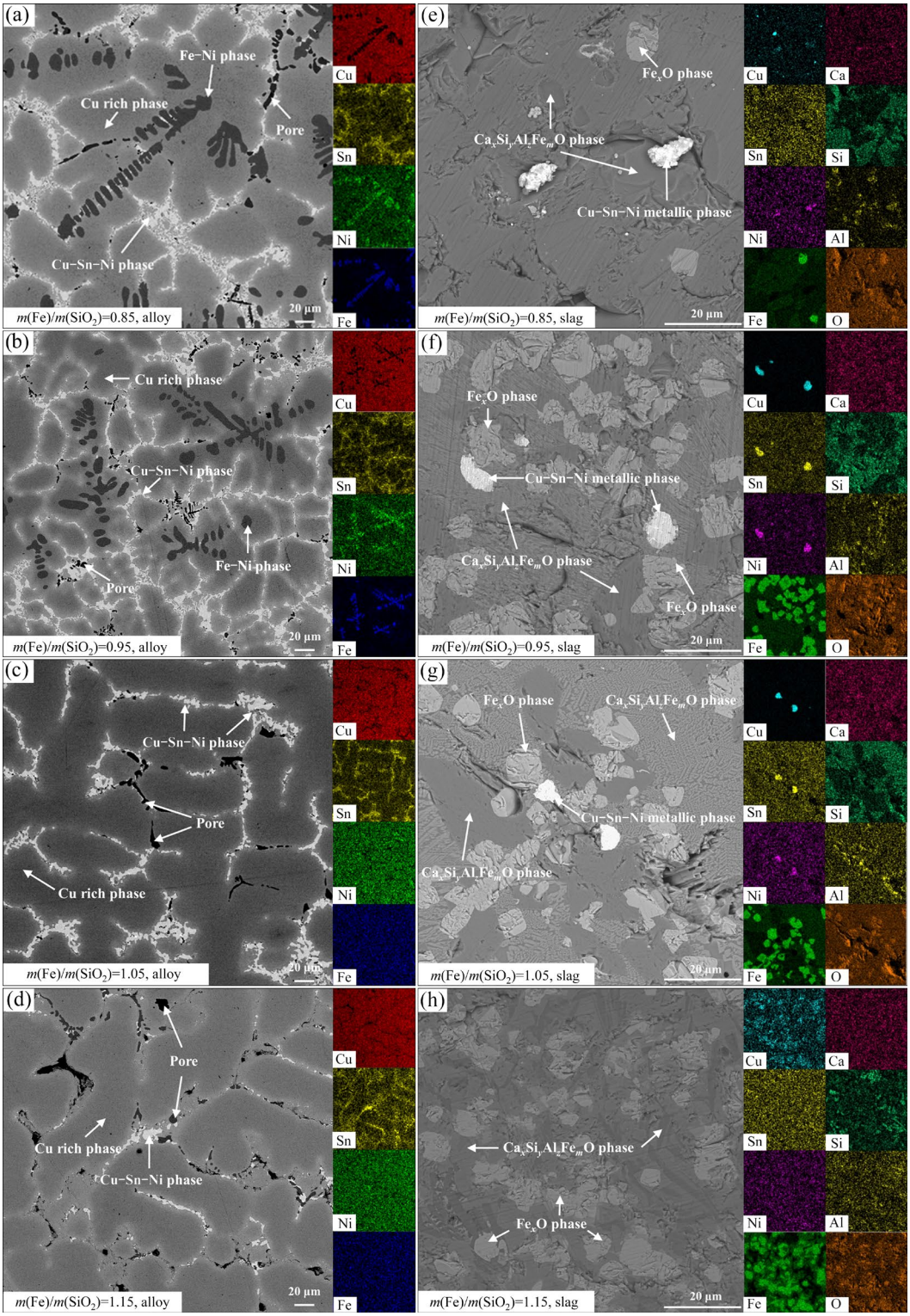

Fig. 12 BSE and EDS images of alloy (a−d) and slag (e−h) at different Fe/SiO_2 ratios

was beneficial to improving the slag properties and reaction efficiency. As seen in Figs. 12(e−h), the slag was mainly composed of silicate phase and Fe_xO phase. The valuable metals were mostly lost in the slag in a Cu−Sn−Ni phase form (a small amount of bright white region in the slag BSE images).

Based on the above analysis, the Fe/SiO_2 ratio of 1.05 was considered to be appropriate. The contents of Cu, Sn and Ni in the alloy were 82.52%, 10.14% and 6.67%, respectively. The quality of the alloy was high, and the impurity Fe content in the

alloy was less than 1%. Most of Cu, Sn and Ni were enriched in the alloy while Fe entered the slag during smelting.

3.3 Thermodynamic equilibrium in smelting process of WPCBs

Figure 13 shows the thermodynamic equilibrium calculation in the smelting process of WPCBs. As seen in Fig. 13(a), between 1100 °C and 1250 °C, the content of Cu, Sn, and Ni did not change significantly, ranging from 82%−85%, 8%−9%, and 7%−8% respectively. These results were consistent with the optimal conditions obtained from previous experimental studies (Cu, Sn and Ni in the alloy were 82.52%, 10.14% and 6.67%, respectively). In addition, within the temperature range studied, the content of Fe was consistently below 1%, indicating that Fe primarily existed in the slag during the smelting process.

As seen from Fig. 13(b), Fe was mainly distributed in the slag within the temperature range of 1100−1250 °C. As the temperature increased from 1100 to 1150 °C, the distribution of Cu, Sn and Ni in the alloy gradually increased. When the temperature exceeded 1150 °C, the distribution of Cu, Sn and Ni in the alloy exceeded 99%. Hence, Cu, Sn and Ni can all enter the alloy phase during smelting. However, this was not consistent with the conclusions drawn from previous experimental studies under optimal conditions, where Cu, Sn and Ni were partially lost in the slag and did not reach the distribution rate calculated by thermodynamic equilibrium. The SEM−EDS analysis of the smelting process slag showed that this was mainly due to the change in the slag properties during smelting, which led to the mechanical entrapment of Cu, Sn and Ni in the slag. Therefore, in order to further improve the direct yield of the alloy, further exploration of the slag properties is needed in the future.

3.4 Mechanism of distribution behavior of valuable metal elements during smelting

Figure 14 illustrates the distribution regularity of elements under different experimental conditions during smelting. It can be seen that the valuable metals were embedded in the slag in the form of metal particles, which decreased the direct yield of valuable metals. The results showed that the direct yield of metals was improved while the purity of alloy decreased significantly with the increase in oxygen-enriched concentration. The increase in oxygen volume can improve the purity of alloy but is not conducive to increasing the direct yield of metals. The increase in CaO/SiO_2 ratio is helpful to improve the direct yield of metals but it affects the quality of the alloy, while the increase in Fe/SiO_2 ratio has little effect on the direct yield of metals.

To sum up, the oxygen-enriched concentration, oxygen volume and slag phase composition (Fe/SiO_2 ratio or CaO/SiO_2 ratio) played dominant roles in the distribution regularity of valuable metals during smelting. However, in order to meet the actual production needs, it is necessary to consider the direct yield of the alloy in order to ensure the high quality of the alloy and realize the sustainable production.

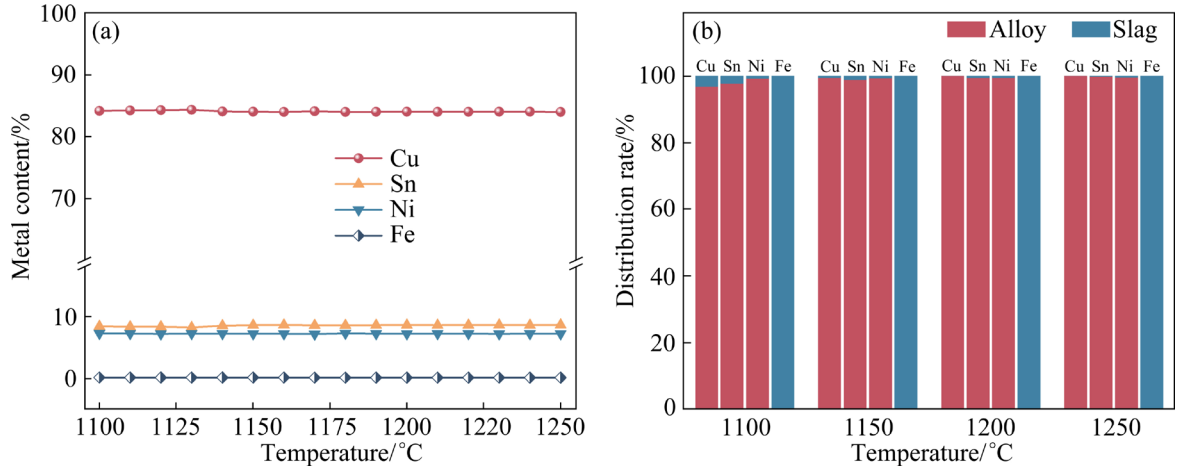

Fig. 13 Thermodynamic equilibrium calculation in smelting process (p_{O_2}=1×10^{-5} Pa): (a) Metal content; (b) Element distribution

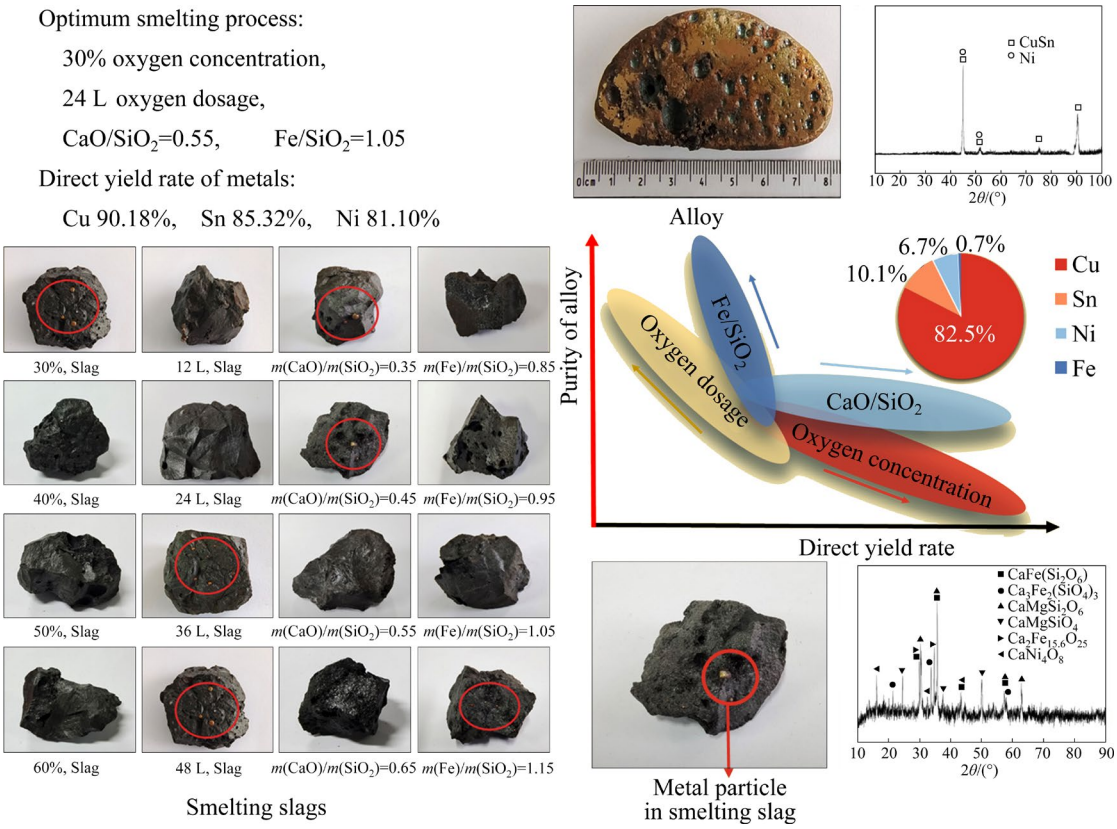

Fig. 14 Distribution regularity of elements under different experimental conditions

4 Conclusions

(1) Under the optimum process conditions, the contents of Cu, Sn and Ni in the alloy were 82.52%, 10.14% and 6.67%, respectively, and the content of Fe was less than 1%. The direct yields of Cu, Sn and Ni were 90.18%, 85.32% and 81.10%, respectively, indicating the effective recovery of valuable metals from WPCBs.

(2) The distribution rates and direct yields of Cu, Sn and Ni as well as the content of impurity Fe in the alloy increased with the increase in oxygen-enriched concentration and CaO/SiO_2 ratio, and the former had a greater influence on the purity of the alloy. The content of impurity Fe in the alloy increases with the decrease in Fe/SiO_2 ratio and the increase in oxygen volume. However, Cu, Sn and Ni easily entered the slag with Fe, which led to the increase in metal loss rate.

(3) Compared to previous works, this study clarifies the distribution behavior of valuable metals in the oxygen-enriched top-blown smelting process of WPCBs, providing theoretical support for further improving the direct yield rate and alloy grade during smelting.

CRediT authorship contribution statement

Kang YAN: Methodology, Investigation, Writing − Original draft; **Wen-can QUAN:** Experimental design and data collection, Data analysis, Software; **Zhong-tang ZHANG:** Writing − Reviewing & editing, Revised manuscript; **Hua-ping NIE, Rui-xiang WANG,** and **Zhi-feng XU:** Supervision, Investigation, Review, Resources.

Declaration of competing interest

The authors declare that they have no known competing financial interests or personal relationships that could have appeared to influence the work reported in this paper.

Acknowledgments

This work was supported by the National Key R&D Program of China (No. 2022YFC2904201), the National Natural Science Foundation of China (Nos. 51904124, 52004111), Jiangxi Provincial Natural Science Foundation, China (Nos. 20224BAB214040, 20232BAB204036), the Program of Qingjiang Excellent Young Talents, Jiangxi University of Science and Technology, China (No. JXUSTQJYX2020012), Jiangxi

Provincial Cultivation Program for Academic and Technical Leaders of Major Subjects, China (Nos. 20212BCJL23052, 20212BCJ23006, 20212BCJ23007), Double Thousand Plan in Jiangxi Province, China (No. jxsq2019201040), and Key Project of Jiangxi Provincial Natural Science Foundation, China (No. 20212ACB204015).

References

[1] D'ADAMO I, FERELLA F, GASTALDI M, MAGGIORE F, ROSA P, TERZI S. Towards sustainable recycling processes: Wasted printed circuit boards as a source of economic opportunities [J]. Resources, Conservation and Recycling, 2019, 149: 455−467.

[2] HUANG Tai-yu, ZHU Jie, HUANG Xiong-fei, RUAN Ju-jun, XU Zhen-ming. Assessment of precious metals positioning in waste printed circuit boards and the economic benefits of recycling [J]. Waste Management, 2022, 139, 105−115.

[3] MIR S, DHAWAN N. A comprehensive review on the recycling of discarded printed circuit boards for resource recovery [J]. Resources, Conservation and Recycling, 2022, 178: 106027.

[4] NEKOUEI R K, TUDELA I, PAHLEVANI F, SAHAJWALLA V. Current trends in direct transformation of waste printed circuit boards (WPCBs) into value-added materials and products [J]. Current Opinion in Green and Sustainable Chemistry, 2020, 24: 14−20.

[5] CHEN Bin, HE Jie, XI Yao-yao, ZENG Xiang-feng, KABAN I, ZHAO Jiu-zhou, HAO Hong-ri. Liquid-liquid hierarchical separation and metal recycling of waste printed circuit boards [J]. Journal of Hazardous Materials, 2019, 364, 388−395.

[6] PANDA R, JADHAO P R, PANT K K, NAIK S N, BHASKAR T. Eco-friendly recovery of metals from waste mobile printed circuit boards using low-temperature roasting [J]. Journal of Hazardous Materials, 2020, 395: 122642.

[7] PENG Zhi-wei, WANG Jie, ZHANG Xin, YAN Jia-xing, SHANG Wen-xing, YU Jing-feng, ZHU Guang-yan, RAO Ming-jun, LI Guang-hui, JIANG Tao. Enrichment of heavy metals from spent printed circuit boards by microwave pyrolysis [J]. Waste Management, 2022, 145: 112−120.

[8] YAN Kang, LIU Chong-wei, LIU Li-ping, XIONG Min, CHEN Jiong-tong, ZHANG Zhong-tang, ZHONG Shui-ping, XU Zhi-feng, HUANG Jin-di. Pyrolysis behaviour and combustion kinetics of waste printed circuit boards [J]. International Journal of Minerals, Metallurgy and Materials, 2022, 29(9): 1722−1732.

[9] YAO Ya-ke, ZHOU Kui, HE Jing-feng, ZHU Ling-tao, ZHAO Yue-min, BAI Qiang. Efficient recovery of valuable metals in the disposal of waste printed circuit boards via reverse flotation [J]. Journal of Cleaner Production, 2020, 284: 124805.

[10] LIU Kang, WANG Meng-meng, TSANG D C W, LIU Li-li, TAN Quan-yin, LI Jin-hui. Facile path for copper recovery from waste printed circuit boards via mechanochemical approach [J]. Journal of Hazardous Materials, 2022, 440: 129638.

[11] HUANG Yu-fong, PAN Meng-wei, LO Shang-lien. Hydrometallurgical metal recovery from waste printed circuit boards pretreated by microwave pyrolysis [J]. Resources, Conservation and Recycling, 2020, 163: 105090.

[12] MARRA A, CESARO A, BELGIORNO V. Separation efficiency of valuable and critical metals in WEEE mechanical treatments [J]. Journal of Cleaner Production, 2018, 186: 490−498.

[13] LI Huan, EKSTEEN J, ORABY E. Hydrometallurgical recovery of metals from waste printed circuit boards (WPCBs): Current status and perspectives—A review [J]. Resources, Conservation and Recycling, 2018, 139: 122−139.

[14] GÁMEZ S, GARCÉS K, TORRE E D L, GUEVARA A. Precious metals recovery from waste printed circuit boards using thiosulfate leaching and ion exchange resin [J]. Hydrometallurgy, 2019, 186: 1−11.

[15] LI Huan, ORABY E, EKSTEEN J. Extraction of precious metals from waste printed circuit boards using cyanide-free alkaline glycine solution in the presence of an oxidant [J]. Minerals Engineering, 2022, 181: 107501.

[16] GUO Xue-yi, QIN Hong, TIAN Qing-hua, LI Dong. Recovery of metals from waste printed circuit boards by selective leaching combined with cyclone electrowinning process [J]. Journal of Hazardous Materials, 2020, 384: 121355.

[17] GUO Xue-yi, TIAN Miao, WANG Song-song, YAN Shu-yang, WANG Qin-meng, YUAN Zhong-sen, TIAN Qing-hua, TANG Ding-xuan, LI Zhong-chen. Element distribution in oxygen-enriched bottom-blown smelting of high-arsenic copper dross [J]. JOM, 2019, 71: 3941−3948.

[18] ZHANG Zhong-tang, DAI Xi. Effect of Fe/SiO_2 and CaO/SiO_2 mass ratios on metal recovery rate and metal content in slag in oxygen-enriched direct smelting of jamesonite concentrate [J]. Transactions of Nonferrous Metals Society of China, 2020, 30(2): 501−508.

[19] ZHANG Jia-liang, HU Jun-tao, ZHANG Wen-juan, CHEN Yong-qiang, WANG Cheng-yan. Efficient and economical recovery of lithium, cobalt, nickel, manganese from cathode scrap of spent lithium-ion batteries [J]. Journal of Cleaner Production, 2018, 204: 437−446.

[20] LIU Chong-wei. Experimental research on thermal decomposition kinetics and synergistic smelting of waste printed circuit boards [D]. Ganzhou: Jiangxi University of Science and Technology, 2021. (in Chinese)

[21] WEN Xiao-chun, WANG Jin-liang, WANG Hou-qing. The distribution behavior of elements during the top-blowing smelting process of electronic waste [J]. Metals, 2021, 11(10): 1615.

[22] YANG Tian-zu, XIAO Hui, CHEN Lin, CHEN Wei, LIU Wei-feng, ZHANG Du-chao. Element distribution in the oxygen-rich side-blow bath smelting of a low-grade bismuth-lead concentrate [J]. JOM, 2018, 70: 1005−1010.

[23] ZHANG Zhong-tang, YAN Kang, NIE Hua-ping, WANG Rui-xiang, XU Zhi-feng. Fundamental theory on pyrometallurgy direct smelting of waste printed circuit boards [J]. JOM, 2021, 73(8): 2549−2557.

[24] GUO Jian-bin, CHEN Zheng, HUANG Wen, DING Zhi-guang. Theoretical research on slag type of top blowing furnace treating waste printed circuit boards [J]. Nonferrous Metals (Extractive Metallurgy), 2021, 11: 15−20. (in Chinese)
[25] CHEN Min, AVARMAA K, KLEMETTINEN L, O'BRIEN H, SHI Jun-jie, TASKINEN P, LINDBERG D, JOKILAAKSO A. Precious metal distributions between copper matte and slag at high P_{SO2} in WEEE reprocessing [J]. Metallurgical and Materials Transactions B, 2021, 52(2): 871−882.
[26] CHEN Min, AVARMAA K, TASKINEN P, KLEMETTINEN L, MICHALLIK R, O'BRIEN H, JOKILAAKSO A. Handling trace elements in WEEE recycling through copper smelting-an experimental and thermodynamic study [J]. Minerals Engineering, 2021, 173: 107189.
[27] WAN Xing-bang, FELLMAN J, JOKILAAKSO A, KLEMETTINEN L, MARJAKOSKI M. Behavior of waste printed circuit board (WPCB) materials in the copper matte smelting process [J]. Metals, 2018, 8(11): 887.
[28] WAN Xing-bang, TASKINEN P, SHI Jun-jie, KLEMETTINEN L, JOKILAAKSO A. Reaction mechanisms of waste printed circuit board recycling in copper smelting: The impurity elements [J]. Minerals Engineering, 2021, 160: 106709.
[29] LIU Tong-yu, MA Tian-yu, LI Ying-min, REN Yu-yan, LIU Wei-hua. Stabilities, mechanical and thermodynamic properties of Al−RE intermetallics: A first-principles study [J]. Journal of Rare Earths, 2022, 40(2): 345−352.
[30] HARVEY J P, LEBREUX-DESILETS F, MARCHAND J, OISHI K, BOUARAB A F, ROBELIN C, GHERIBI A E, PELTON A D. On the application of the FactSage thermochemical software and databases in materials science and pyrometallurgy [J]. Processes, 2020, 8(9): 1156.

废旧线路板富氧顶吹熔炼过程中有价元素的分布行为

严 康[1,2,3]，全温灿[1,2,3]，张忠堂[1,2,3]，聂华平[1,2,3]，王瑞祥[1,2,3]，徐志峰[2,3,4]

1. 江西理工大学 冶金工程学院，赣州 341000；
2. 自然资源部 离子型稀土资源与环境重点实验室，赣州 341000；
3. 赣州市绿色冶金与过程强化工程技术研究中心，赣州 341000；
4. 江西应用技术职业学院 材料工程学院，赣州 341000

摘 要：采用富氧顶吹熔炼技术处理废旧线路板是一种是非常有前途的工艺。系统研究熔炼过程中富氧浓度、通氧量、CaO/SiO_2 (质量比)和 Fe/SiO_2 (质量比)对有价金属分布行为的影响，通过单因素条件实验确定最优工艺参数。结合 XRD、SEM−EDS 和 ICP-AES 等检测手段，对熔炼过程产出合金和炉渣进行化学物相、赋存形态及化学元素进行表征和分析。结果发现，熔炼过程中 Cu、Sn 和 Ni 元素主要赋存在合金中，而 Fe 元素主要被氧化入渣。在温度为 1250 ℃，富氧浓度为 30%，通氧量为 24 L，CaO/SiO_2 质量比为 0.55 和 Fe/SiO_2 质量比为 1.05 条件下，Cu、Sn 和 Ni 的直收率可分别达到 90.18%、85.32%和 81.10%。实验结果表明熔炼过程有价金属主要是以机械夹杂方式损失于渣中。

关键词：废旧线路板；顶吹熔炼；元素分布；热力学分析；渣型

(Edited by Xiang-Qun LI)